

1 **Measurement report: Lessons learned from the comparison**
2 **and combination of fine carbonaceous aerosol source**
3 **apportionment at two locations in the city of Strasbourg,**
4 **France**

5 Hasna Chebaicheb^{1,2,3}, Mélodie Chatain⁴, Olivier Favez^{2,3}, Joel F. de Brito¹, Vincent Crenn⁵,
6 Tanguy Amodeo^{2,3}, Mohamed Gherras², Emmanuel Jantzem⁴, Caroline Marchand^{2,3},
7 Véronique Riffault^{1,3}

8 ¹IMT Nord Europe, Institut Mines-Télécom, Université de Lille, Centre for Energy and Environment, 59000,
9 Lille, France

10 ²Institut National de l'environnement Industriel et des Risques (INERIS), 60550 Verneuil-en-Halatte, France

11 ³Laboratoire Central de Surveillance de la Qualité de l'Air (LCSQA), 60550 Verneuil-en-Halatte, France

12 ⁴Atmo Grand Est, 67300 Schiltigheim, France

13 ⁵ADDAIR, F-78530 Buc, France

14 *Correspondence to:* Hasna Chebaicheb (hasna.chebaicheb@ineris.fr); Mélodie Chatain (melodie.chatain@atmo-grandest.eu)

15

16 **Abstract.** Source apportionment analyses of carbonaceous aerosol were conducted at two neighboring urban sites
17 in Strasbourg, France, during the winter of 2019/2020 using ACSMs (Aerosol Chemical Speciation Monitors; for
18 non-refractory submicron aerosols), aethalometers (AE33; for equivalent Black Carbon - eBC) and filter-based
19 offline chemical speciation. Positive Matrix Factorization (PMF) was applied to organic aerosols (OA) following
20 two strategies: i) analyzing each site individually, ii) combining both sites into a single dataset. Both methods
21 resolved five OA factors: hydrocarbon-like (HOA), biomass burning (BBOA), cooking-like (COA-like),
22 oxygenated (OOA), and an amine-related OA (58-OA) factor. The latter factor, accounting for ~4% of the total
23 OA mass at each site, showed clear diel profiles and a distinct origin marked by specific wind directions,
24 suggesting a unique local source, potentially linked to industrial emissions. The present study also highlights the
25 challenge of attributing a cooking-only origin to the COA-like factor, which exhibited a diel cycle similar to
26 biomass burning OA at the background site. The combined PMF analysis improved the apportionment of cooking
27 emissions at nighttime, especially for the traffic site, compared to individual PMF analyses, but it did not enhance
28 the other OA factors due to instrumental specificities (i.e., different fragmentation patterns) leading to differences
29 in OA mass spectra between the two instruments. Overall, this study argues for careful inspection of instrumental
30 peculiarities in ACSM and AE33 data treatment and provides hints to benefit from their use at various locations
31 at the city scale. It also allows comparison between different types of PMF analyses, showing that combined PMF
32 may not be appropriate for improving the consistency of OA factors in some cases such as the one presented here.

33 **Keywords.** Urban pollution, PMF, organic aerosols, Amine-related OA

Définition du style : Police par défaut

a mis en forme : Anglais (États-Unis)

37 **1 Introduction**

38 Air pollution influences climate change and induces adverse effects on human health, increasing disease and
39 mortality rates (EEA, 2022). In particular, particulate matter such as those with an aerodynamic diameter smaller
40 than 1 μm (PM_1) are inhaled and reach the deeper respiratory system, leading to a range of health problems
41 including respiratory and cardiovascular disorders, disruptions in reproductive and central nervous functionalities,
42 as well as the development of cancer (WHO, 2022; Duarte et al., 2023). Identifying their chemical composition
43 and main emission sources has become a priority for air quality (AQ) agencies to build up and assess efficient
44 abatement strategies. Improving knowledge of their geographical origins is also a major challenge to better adapt
45 local policies in a larger regional scale context.

46 In France, regional air quality monitoring networks (AQMN) and the national reference laboratory (termed
47 'LCSQA') are operating the CARA program for *in situ* observation of the PM chemical composition in urban
48 environments and subsequent source apportionment studies (Favez et al., 2021). Chebaicheb et al. (2024) recently
49 analyzed and discussed long-term (> 1 year) measurements of fine particles using online instruments at 13 CARA
50 sites, providing PM_1 chemical composition, with annual mean loadings ranging from 7 to 16 $\mu\text{g m}^{-3}$ in French
51 urban background environments. This concentration range is relatively low compared to other cities outside
52 Europe but still exceeds the World Health Organization (WHO) recommended annual concentration limit of 5 μg
53 m^{-3} for $\text{PM}_{2.5}$. Organic aerosols (OA) represent a major fraction of the total PM_1 mass (40-60 %), a trend
54 commonly observed worldwide (Bressi et al., 2021; Chen et al., 2022; Li et al., 2022; Via et al., 2021; Zhou et al.,
55 2020).

56 Identifying the sources of the complex mix comprising the OA fraction is therefore crucial to develop effective
57 mitigation strategies and improve AQ. Source apportionment (SA) approaches, including receptor models, have
58 been widely used in urban AQ research during the last decades. In particular, Positive Matrix Factorization (PMF),
59 as introduced by Paatero and Tapper (1994), stands out as one of the most extensively utilized tools (Hopke et al.,
60 2020). PMF can be applied to various types of datasets, typically obtained from offline chemical analyses of filter
61 samples or from online characterization of the aerosol chemistry and/or physical properties. Knowledge of OA
62 chemistry and sources has greatly benefited from the development of aerosol mass spectrometry and subsequent
63 application of PMF-type analysis to organic mass spectra since the mid-2000s (Crippa et al., 2014). This
64 commonly allows to feature different families of organic compounds originating from primary emissions -
65 typically, biomass burning OA (BBOA), hydrocarbon-like OA (HOA), cooking-like OA (COA) - or from various
66 oxidation processes, e.g., leading to less- or more-oxidized oxygenated OA (LO-OOA and MO-OOA,
67 respectively). Chen et al. (2022) recently proposed and applied a common protocol for advanced PMF analysis
68 on unit-mass resolution (UMR) organic mass spectra obtained from long-term measurements at 22 European sites.
69 This protocol is based on the use of the multi-linear engine (ME-2), allowing to introduce *a priori* knowledge (or
70 assumption) on the mass spectral fingerprint of some OA factors to facilitate the comparison of SA outputs
71 obtained at different locations. Such a standard methodology might also be of particular interest when conducting
72 a SA study at the city scale to estimate increments due to local emissions on top of regional and/or urban
73 background air pollution. Furthermore, previous studies also proposed to combine neighboring sites on a unique
74 PMF analysis, in order to reinforce the consistency of the comparison of SA results obtained for each site. Such a
75 multisite PMF analysis is considered to potentially improve the outputs' robustness, enhancing the variability in
76 the resulting input dataset when using larger dataset than individual PMF (e.g., Pandolfi et al., 2020). To our
77 knowledge, such a combined approach has been only applied to filter-based offline measurements, and not to
78 aerosol mass spectrometry datasets.

79 In a previous paper, Chatain et al., (2021) compared the particle size distribution and aerosol concentrations
80 between an urban background site and a roadside site during winter 2019/2020 in Strasbourg, France, showing
81 higher particle number concentrations and particles smaller than 100 nm at the latter site compared to the former
82 throughout the observation period. This measurement campaign also included simultaneous monitoring of black
83 carbon (BC) and non-refractory submicron chemical species (NR- PM_1) at both sites, allowing for the investigation
84 of major factors contributing to fine aerosols. In this context, this manuscript focuses on a SA study to analyze
85 the main origins of carbonaceous species at two nearby sites located 2.5 km apart in Strasbourg. In order to
86 compare the PMF results obtained for OA between these neighboring sites, a two-fold approach was undertaken.
87 Initially, a standard PMF analysis was conducted independently for each site but in a harmonized way (i.e. using
88 the same constraints and criteria). Subsequently, considering the geographical proximity of the sites, a combined
89 PMF analysis was also carried out. Thus, the present study notably assesses the reliability and consistency of the
90 results obtained from the individual PMF outputs compared with the combined ones. This comparative assessment
91 also aims at discerning the main sources of pollution at these closely related sites.

92 **2 Methodology**

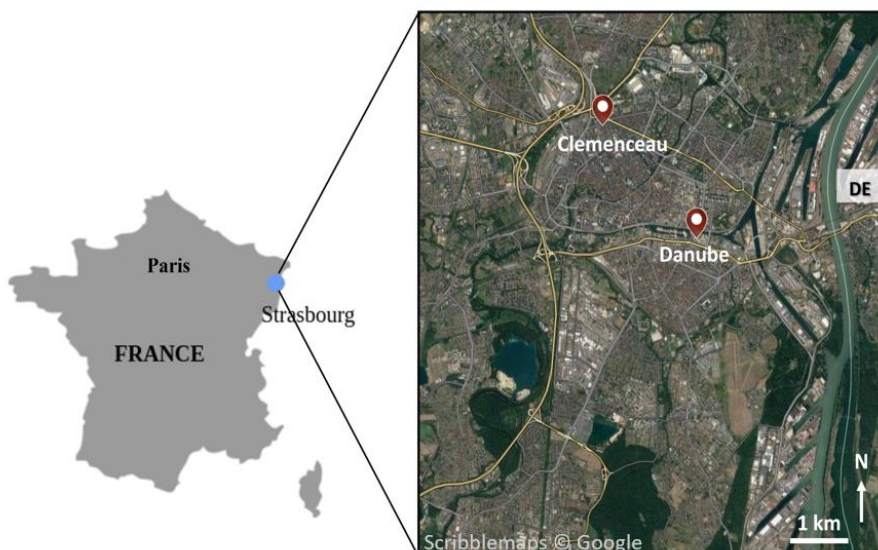
93 **2.1 Sampling sites**

94 The city of Strasbourg is located at the edge of North-Eastern France, connecting with Germany, along the river
95 Rhine. It is part of the most populous urban area in France and the largest on a regional scale. It is highly urbanized
96 and crossed by several major roads, including the north-south axis (A35-A4 motorway) and the east-west axis
97 (Rhine Avenue). Residential and commercial areas are adjacent to major industrial areas to the east and south,
98 and the entire urban area is surrounded by agricultural land.

99 Despite significant improvements in AQ in recent decades, Strasbourg still experiences more than ten days per
100 year with PM_{10} levels exceeding the daily limit value of $50 \mu g m^{-3}$ set by the European Directive 2008/50/CE. In
101 addition, in 2022, 100 % of the population lived in an area exceeding the WHO guideline for the annual $PM_{2.5}$
102 average (ATMO Grand Est, 2023). Moreover, the city can be significantly influenced by air masses from central
103 Europe under anticyclonic conditions, as already observed for other urban areas in northern France, such as
104 Greater Paris (MEGAPOLI, e.g., Beekmann et al. 2015; Freutel et al., 2013) and Lille (Chebaicheb et al., 2023).

105 A detailed description of the two sites (background and roadside) investigated here can be found in Chatain et al.
106 (2021). Briefly, both sites correspond to fixed stations operated by the ATMO Grand Est AASQA
107 (<http://www.atmo-grandest.eu>). The first one (called Danube) corresponds to an urban background station located
108 southwest of the city center of Strasbourg (Figure 1). This station was installed at the center of a recently built
109 eco-district between a small canal (Bassin Dusuzeau) and the Rhine Avenue. The second site (called Clemenceau)
110 corresponds to an urban roadside station located at the corner of an intersection between two major roads in the
111 north of the city center of Strasbourg.

Code de champ modifié



112

113 **Figure 1: Location of the two sites: Strasbourg Danube, and Strasbourg Clemenceau.**

114 **2.2 Measurements**

115 All the measurements at both sites were carried out by ATMO Grand Est. These measurements include regulatory
116 monitoring of PM using a fine dust aerosol spectrometer (FIDAS 200, Palas GmbH) measuring the optical light
117 scattering of singles particles, and demonstrated to be equivalent to the gravimetric reference method for PM_{10}

118 and $\text{PM}_{2.5}$ (NF EN 12341); as well as NO_x using the chemiluminescence method (APNA-370, Horiba) as
119 recommended by the NF EN 14211 reference method.

120 During winter 2019/2020, the chemical composition of NR- PM_1 was investigated using two quadrupole ACSMs
121 (Q-ACSM, *Aerosol Chemical Speciation Monitor*, Ng et al., (2011)) concomitantly at the Danube and Clemenceau
122 stations. In this instrument, atmospheric particles are sampled at a flow rate of 3 L min^{-1} (sampling line OD = 9.5
123 mm; ID = 6.5 mm; 2.2 m long stainless tube) with a cut-off at $2.5 \mu\text{m}$ using a sampling head, then subsampled at
124 a flow rate of around 85 cc min^{-1} determined by a $100 \mu\text{m}$ critical aperture mounted at the instrument inlet.
125 equipped with PM_1 aerodynamic lens. The submicron particles are then focused by an aerodynamic lens system
126 toward a tungsten vaporizer heated at 600°C under vacuum. The non-refractory constituents of particles are
127 vaporized and then electronically ionized (70 eV). The resulting fragments are separated by a quadrupole
128 depending on their mass-to-charge ratio (m/z) operating in a scanning mode from $m/z = 10$ to 150. The signal
129 intensity (in Amps) proportional to the total amount of ions hitting the detector (SEM: Secondary Electron
130 Multiplier) for each m/z is then used to obtain the raw mass spectra. The final concentrations of OA, nitrate (NO_3),
131 sulfate (SO_4), ammonium (NH_4), and chloride (Cl) are obtained using a fragmentation table (Allan et al., 2004).
132 Roughly, inorganic compounds are first quantified based on their fragmentation patterns, and the remaining signal
133 at each m/z is attributed to organic fragments, forming the measured organic fraction. The resulting OA mass
134 spectra can then be used as an input matrix, along with its corresponding uncertainties matrix, for PMF analysis.
135 A critical point for the calculation of the species mass concentrations is the determination of their ionization
136 efficiencies. This is basically done by taking nitrate as the reference (since it has a rather simple fragmentation
137 pattern and few interferences at its specific m/z fragments) and then measuring or assuming specific relative
138 ionization efficiency (RIE) values relative to the NO_3 response factor (RF) for other species. In the present study,
139 RF, RIE_{NH_4} , and RIE_{SO_4} were determined by on-site calibrations during the measurement campaign, and the
140 commonly-used default RIE values of 1.4 and 1.3 were used for OA and Cl, respectively, for both ACSM datasets.
141 The ACSM species were corrected using composition-dependent collection efficiency (CDCE) correction, by
142 applying the Middlebrook algorithm (Middlebrook et al., 2011), with a minimum CE of 0.5.

143 It is also worth noting that the two ACSMs deployed here were previously compared (August-October 2019) at a
144 suburban background station of a nearby city (Metz-Borny, France), showing very satisfactory agreement for NO_3
145 measurements (~100%) but substantial differences - of about 30% at the highest concentration ranges - in OA
146 (and SO_4) measurements (Fig. S1). These differences did not appear to be influenced by discrepancies in relative
147 ion transmission (RIT) as the corresponding correction curves, based on the naphthalene internal standard
148 fingerprint, behaved as generally expected for ACSM devices (Fig. S2), and the highest differences were already
149 observed at the lowest m/z (Fig. S3). They are also unlikely to be related to differences in RIE since both
150 instruments were sampling the same ambient air and IE values led to a satisfactory agreement for nitrate
151 measurements (slope: 1.05; $r^2 = 0.96$, Fig. S1), except if the variations of organic RIE with the aerosol oxidation
152 state (Katz et al., 2021; Nault et al., 2023; Xu et al., 2018) might also be instrument-specific. As a matter of fact,
153 the few m/z ratios showing the highest concentrations for the under-estimating instrument – which was further
154 installed at the Clemenceau station during the wintertime Strasbourg campaign – included m/z commonly
155 attributed to biomass burning OA (in particular m/z 60 and 73, see Fig. S3). It should also be noted that no Pieber-
156 like artifact (Pieber et al., 2016) was observed during ammonium nitrate or ammonium sulfate calibrations.
157 Moreover, the voltage applied to the vaporizers in both instruments was kept at the values determined for each of
158 them by the manufacturer, theoretically ensuring a similar vaporizer temperature of about 600°C in the two
159 ACSM. In this context, besides any possible differences in lens transmission efficiencies, no other instrumental
160 bias could be suspected to explain the discrepancies observed in OA measurements during this pre-campaign
161 intercomparison exercise.

162 For the winter campaign, both Strasbourg sites were also equipped with a multi-wavelength Aethalometer (AE33,
163 Magee Scientific), using a sampling head with a cut-off diameter of $2.5 \mu\text{m}$ at a flow rate of 5 L/min (sampling
164 line OD = 12.7 mm; ID = 10.8 mm; 1.8 m long stainless tube and 2.5 m static dissipative tubing). A full description
165 of the AE33 operating principles is given by Drinovec et al. (2015). Briefly, it is based on the measurement of
166 optical attenuation in order to determine aerosol absorption coefficients (b_{abs}) at selected wavelengths. Aerosols
167 are continuously sampled onto a filter tape, causing a decrease of light transmission through the sampled filter
168 spot(s) which is compared to the light transmission through an unsampled area of the filter tape. In the AE33
169 model, optical measurements are conducted at seven optical wavelengths ranging from near-ultraviolet (UV) to
170 near-infrared (IR) (370, 470, 525, 590, 660, 880, and 950 nm), and sampling artifacts known as filter-loading
171 effect are corrected thanks to the dual-spot technology (Drinovec et al., 2015). By convention for multi-
172 wavelength aethalometer, equivalent Black Carbon (eBC) is derived from measurements at 880 nm, assuming a
173 mass absorption cross-section (MAC) value, such as:

174
$$eBC = b_{abs,880nm} / MAC_{880nm}$$

Eq. (1)

175 In line with the current ACTRIS guidelines, $b_{abs,880nm}$ was obtained applying a filter type-dependent harmonization
176 factor (1.76 for the MF8060 filter tape used here) to account for multiple scattering effects, and a MAC value of
177 $7.5 \text{ m}^2 \text{ g}^{-1}$ at 880 nm was considered to estimate eBC concentrations (<https://actris-ecac.eu/particle-light-absorption.html>).

Code de champ modifié

179 All these measurements underwent regular quality checks, including calibration and preventive maintenance,
180 following the manufacturer's recommendations, ACTRIS standard operating procedures, and guidelines provided
181 by ACMCC (Aerosol Chemical Monitor Calibration Center) in the ACTRIS framework (Laj et al., 2024) and by
182 the LCSQA at the national level. Quality control was routinely achieved following daily and weekly technical
183 validation procedures, supplemented by a monthly environmental validation investigation. Finally, data handling
184 procedures defined in Chebaicheb et al. (2024) data were applied to ACSM and AE33 datasets.185 In addition, quartz fiber filters (TissuQuartz, Whatman, 47 mm diameter) pre-heated at 500°C during 4 hours and
186 Leckel samplers (model SEQ 47/50) running at 2.3 m³/h were used to collect daily PM₁ samples simultaneously
187 at both sites from 4 to 29 February 2020 for offline analyses of organic carbon (OC) and elemental carbon (EC)
188 using a Sunset Lab instrument and following the EUSAAR-2 thermo-optical protocol (Cavalli et al., 2010). Daily
189 mean values obtained for eBC and OA (from AE33 and ACSM, respectively) were then compared to EC and OC
190 offline measurements, respectively. Results showed very good correlation coefficient values for both comparisons
191 ($r^2 > 0.9$, Fig. S4S5) with OA-to-OC ratios (about 1.4) in the lower range of what is commonly observed in urban
192 environments (e.g., Aitken et al., 2008). This may be linked to the predominance of primary organic aerosols
193 (from various combustion processes), which are less oxidized than secondary OA (SOA). This could also be partly
194 related to possible OC overestimations due to positive sampling artifacts - e.g., adsorption of semi-volatile organic
195 compounds onto the filter (e.g., Kim et al., 2001) - and/or OA underestimation from ACSM measurements, for
196 instance due to poor lens transmission efficiency at the entrance of the ACSM for the finest and/or largest particles
197 within the submicron aerosol fraction (e.g., Liu et al., 2007). Nevertheless, the consistency obtained for OA-to-
198 OC ratio values with both ACSMs comforts the comparability of ACSM results.199 The three measurement instruments, AE33, ACSM, and FIDAS are located in the same station and therefore in
200 exactly the same place. Their sampling lines are separate but only a few meters apart, in accordance with national
201 guidelines, and are set at the same sampling height. The ACSM and AE33 instruments were equipped with a dryer
202 to maintain a relative humidity below 40 %.203

2.3 eBC source apportionment

204 Following Sandradewi et al. (2008), multi-wavelength absorption measurements can be used to deconvolve eBC
205 into two main fractions, classically identified as fossil fuel (eBC_{ff}) and wood burning (eBC_{wb}) components. To do
206 so, it is assumed that the light absorption due to Brown Carbon (BrC) at near UV wavelengths in winter is
207 primarily linked to wood-burning emissions, which has been recently documented by Zhang et al. (2020) at the
208 national scale. More generally, the model allows distinguishing between highly efficient combustion processes
209 (like traffic exhaust emissions) and poor combustion conditions.210 This so-called Aethalometer model is based on the additivity of absorption coefficients from both of these source
211 categories and on their own light absorption spectral fingerprints, such as:

212
$$b_{abs,\lambda} = b_{abs,ff,\lambda} + b_{abs,wb,\lambda}$$
 Eq. (2)

213
$$b_{abs,wb,470nm} / b_{abs,wb,950nm} = (470/950)^{\alpha_{wb}}$$
 Eq. (3)

214
$$b_{abs,ff,470nm} / b_{abs,ff,950nm} = (470/950)^{\alpha_{ff}}$$
 Eq. (4)

215 where α_{ff} and α_{wb} stand for the Absorption Ångström Exponent (AAE) of the fossil fuel and wood burning
216 fractions, respectively. These parameters have initially been set to default values of 1 and 2, respectively
217 (Sandradewi et al., 2008; Drinovec et al., 2015). However, further studies illustrated that the choice of these
218 parameters is highly critical for the consistency of the Aethalometer model outputs so that site-specific values
219 should preferably be determined (e.g., Favez et al., 2010; Zotter et al., 2017; Savadkoohi et al., 2023). Following
220 Tobler et al. (2021), α_{ff} has been defined here as the first percentile of AAE values measured for ambient air
221 particles during the campaign, applying a stringent data point selection based on the determination coefficient (r^2

222 > 0.99) obtained from the fit of the b_{abs} spectral dependence ($b_{abs,\lambda}$ vs. λ). Once α_{ff} was set for both sites (at 1.00
 223 and 1.06 for Danube and Clemenceau, respectively), the optimal α_{wb} values could be investigated based on the
 224 results of a sensitivity study aiming at optimizing correlation coefficients between eBC_{wb} and m/z 60 signal
 225 (commonly used as a biomass burning tracer) from ACSM measurements while keeping the correlation between
 226 eBC_{ff} and m/z 60 as low as possible. On the other hand, the correlation between eBC_{ff} and NO concentration
 227 (considered as a proxy for road traffic exhaust emission) allows to determine the minimum α_{wb} . To be coherent,
 228 the correlation between NO and eBC_{ff} must be greater or at least equal to the correlation between NO and eBC_{wb} .
 229 Such a methodology is in line with recommendations also provided by Savadkoohi et al. (2025). This led to the
 230 determination of α_{wb} values of 1.6 and 1.7 for the Clemenceau and Danube sites, respectively, during the studied
 231 period (Fig. [S5S7](#)).

232 **2.4 OA source apportionment**

233 The data derived from the Q-ACSM at both sites were analyzed using the Aerodyne software ‘acsm local’ version
 234 6.37. Both OA concentrations matrices and their error matrices were exported to apply the PMF method using the
 235 Source Finder Pro software (SoFi Pro v8, Datalystica Ltd., Switzerland) with the ME-2 solver within the Igor Pro
 236 software environment (Wave Metrics, Inc., USA). Briefly, the PMF model allows for the separation of the
 237 measured organic concentrations matrix (x_{ij}) at a receptor site into organic mass spectra attributed to “sources”
 238 (profiles f_{kj}) and their contributions over time (time series g_{ik}), along with the residuals (e_{ij}), as described in
 239 equation (5):

$$240 \quad x_{ij} = \sum_{k=1}^p g_{ik} \times f_{kj} + e_{ij} \quad \text{Eq. (5)}$$

241 The objective is to find the number of factors “p” while minimizing a quantity Q defined as the sum of the squares
 242 of the residuals (e_{ij}) on the measurement uncertainties (σ_{ij}):

$$243 \quad Q = \sum_{i=1}^n \sum_{j=1}^m (e_{ij} / \sigma_{ij})^2 \quad \text{Eq. (6)}$$

244 The SoFi Pro software allows the use of the a-value approach to overcome the rotational ambiguity caused by the
 245 application of PMF. This approach helps constrain known factor profiles or time series at the site, using a scalar
 246 a-value varying from 0 to 1, as defined in these equations:

$$247 \quad f_{solution} = f_{reference} (1 \pm a) \quad \text{Eq. (7)}$$

$$248 \quad g_{solution} = g_{reference} (1 \pm a) \quad \text{Eq. (8)}$$

249 The PMF solutions are then evaluated using the bootstrap technique which allows estimating the uncertainties of
 250 the study.

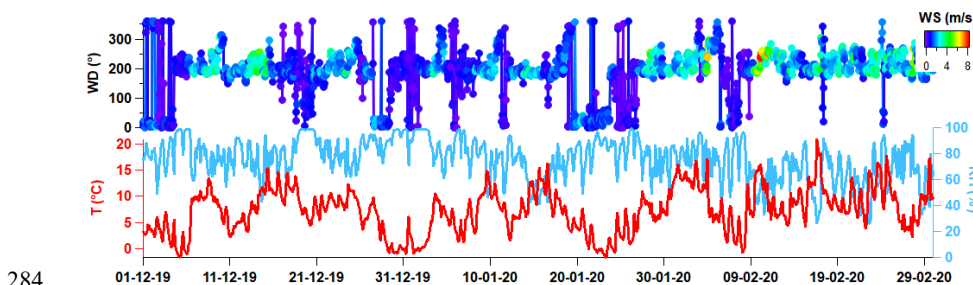
251 A standard PMF analysis was first performed for each site during winter 2019/2020 (December, January,
 252 February; DJF), as detailed in the supplementary information, section S1. Briefly, unconstrained PMF was initially
 253 applied to pre-determine the potential number of factors (2-8 factor tests with ten PMF runs for each number of
 254 factors), allowing to identify five main OA factors at each site, namely one oxygenated (OOA) and four primary
 255 OA factors (hydrocarbon-like OA (HOA), cooking-like factor (COA), biomass burning OA (BBOA), as well as
 256 a specific 58-related OA). Then, a constrained PMF was conducted using the reference profiles from Crippa et
 257 al., (2013) for HOA and COA, which allowed us to obtain BBOA and 58-OA factors for each site without
 258 constraining them. After establishing a reasonable PMF solution for both sites, we applied the bootstrap analysis
 259 to test the stability of the solutions. The average bootstrapped solutions obtained at both sites are presented and
 260 discussed in section 3.

261 An interesting experimental issue is the effect of possible instrumental biases - e.g., as described by Pieber et al.
 262 (2016) - on the obtained SA results. From the comparison of PMF analyses performed on datasets simultaneously
 263 obtained for 14 different ACSMs, Fröhlich et al. (2015) demonstrated that relatively important discrepancies in
 264 the OA mass spectra do not necessarily lead to significant differences in the PMF results from one instrument to
 265 another. An open question remains on the effect of mixing mass spectra datasets from two (or more) distinct
 266 ACSMs in a single input PMF matrix. Such multisite PMF studies have been recently introduced for the combined
 267 analysis of filter-based chemical speciation datasets, which can be obtained from offline analyses using the same
 268 laboratory equipment (e.g., Mooibroek et al., 2011, 2016; Pandolfi et al., 2020), but have rarely, if not never, been

269 presented yet for online ACSM (or AMS) measurements. Considering the unexplained differences in mass spectral
 270 fingerprints observed from co-located measurements during the preliminary intercomparison campaign in Metz
 271 (see above), it appeared of particular interest to test here such a multisite approach combining OA measurements
 272 at both nearby Strasbourg sites in a single PMF input matrix, also verifying the robustness and accuracy of the
 273 individual PMF solutions. This combined PMF consisted of merging the two concentration and error matrices
 274 from the two sites vertically with the same number of variables (m/z up to 100) and averaging the two-time series
 275 over 30 min. As for standard independent PMF analyses, the HOA and COA factors were constrained using
 276 Crippa's reference mass spectra. Bootstrap analysis and selection criteria were then applied to obtain the final
 277 solution as presented in SI, section S2.

278 2.5 Meteorological data and wind analysis

279 Meteorological parameters have been measured at a background site located a few kilometers northwest of the
 280 study sites. Temperature (T) and relative humidity (RH) were measured by dedicated probes (HMP Vaisala model)
 281 and wind data (speed, WS; and direction, WD) by a wind vane (TAVID Chauvin Arnoux model). As presented
 282 in Figure 2, the investigated period was dominated by south-western and relatively warm (5-10°C) air masses,
 283 except during relatively short colder periods (e.g., around New Year and 22 Jan.) with northern winds.



284 285 **Figure 2: Meteorological parameters in Strasbourg during winter 2019/2020.**

286 In order to understand the origin of air pollutants, wind and trajectory analyses were conducted, coupling pollutant
 287 concentrations with meteorological parameters (wind speed and direction) by computing the Non-parametric
 288 Wind Regression (NWR) model using the Zefir tool (Petit et al., 2017a), also allowing to qualitatively differentiate
 289 between local and regional eBC and OA origins according to wind speed.

290 3 Chemical composition

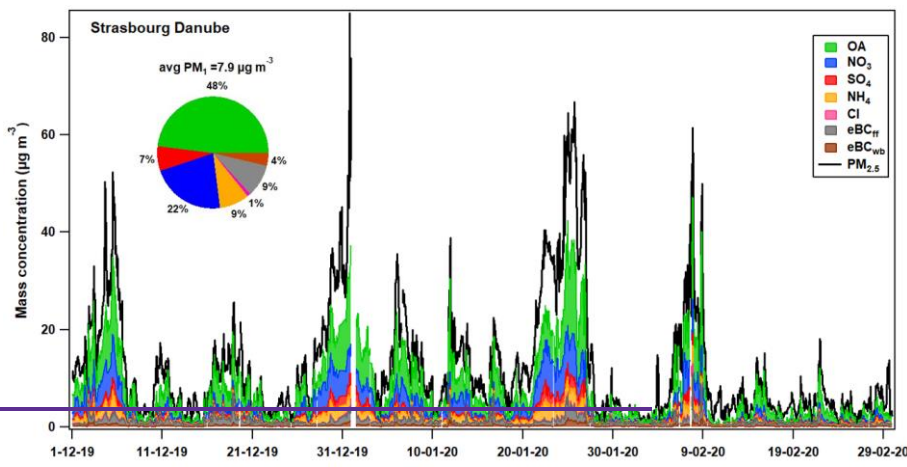
291 Online chemical measurements could be validated by comparison with co-located regulatory PM_{2.5} measurements.
 292 In this chemical mass closure exercise, NR-PM₁ is first calculated as the sum of the five chemical species from
 293 ACSM: OA, NO₃, SO₄, NH₄, and Cl. The PM₁ concentration is then approximated by adding eBC to NR-PM₁ and
 294 further compared with the mass concentration of PM_{2.5} measured by the FIDAS instrument at both sites. Results
 295 indicate that ACSM and AE33 measurements together account for 62 % and 75 % of PM_{2.5}, with coefficients of
 296 determination (r^2) equal to 0.90 and 0.87 for the Danube and Clemenceau sites, respectively (Fig. S6S8).

297 Figure 3 displays the mass concentrations of PM₁ species and the average contribution of eBC, NR-PM₁ species,
 298 and PM_{2.5} during winter 2019/2020 at the Danube and Clemenceau sites. OA dominates the average PM₁ chemical
 299 composition with 48 % and 45 % at the urban background and traffic sites, respectively, as already observed in
 300 previous studies in winter at the national scale in the Paris region (44 %), Lille (37 %) and Dunkirk (34 %)
 301 (Chebaicheb et al., 2024, 2023, Favez et al., 2021; Zhang et al., 2021; Petit et al., 2014). Secondary inorganic
 302 species (NO₃, SO₄, and NH₄) also contribute significantly, accounting for around 40 % of PM₁ total mass, mainly
 303 from NO₃ (22-24 %). These observations are consistent with the regional formation of ammonium nitrate
 304 (NH₄NO₃; AN), which is greater than ammonium sulfate ((NH₄)₂SO₄); AS). NH₃, considered as mainly emitted
 305 by agricultural activities, is expected to react preferentially with sulfur compounds (mainly sulfuric acid (H₂SO₄)
 306 formed from sulfur dioxide (SO₂)). However, regional SO₂ concentrations have been extremely low since the late
 307 2010s (below 1 $\mu\text{g m}^{-3}$ since 2016 at regional background sites). Therefore, AS is mainly derived from long-range
 308 transport in urban areas, and the remaining NH₃ is available to react with NO_x present, notably to form AN locally.

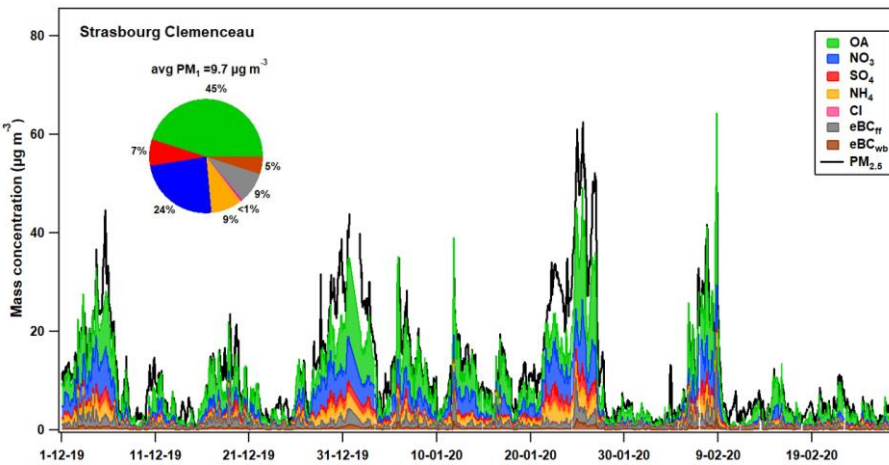
309 However, the balance of AN formation also depends on meteorological conditions (low temperatures, high relative
 310 humidity, high pressure), leading to higher AN concentrations in winter/early spring when these meteorological
 311 conditions are met simultaneously with higher local NH_3 emissions. Previous studies conducted in this part of
 312 Europe, e.g., in Greater Paris (Zhang et al., 2019; Petit et al., 2014) or in the Lille metropolitan area (Chebaicheb
 313 et al., 2023) also highlighted the high contribution of organics and nitrate in PM_{1} particles, as well as the high
 314 impact of transboundary pollution advection from Eastern Europe in northern France for particulate matter
 315 (Waked et al., 2018; Potier et al., 2019).

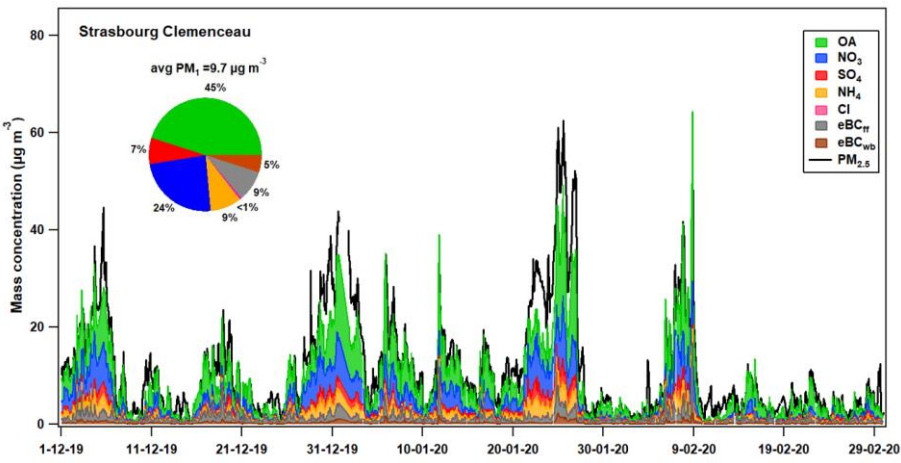
316 Both sites showed a similar high temporal variation, with PM_{1} ranging from a few $\mu\text{g m}^{-3}$ to over $40 \mu\text{g m}^{-3}$ at the
 317 Danube site and over $60 \mu\text{g m}^{-3}$ at the Clemenceau site. The coincidence of the peaks at both sites results from the
 318 strong influence of atmospheric conditions and common local sources. The accumulation of local primary particles
 319 is expected during the coldest periods associated with low wind speed. New Year's event is one of the peaks
 320 associated with elevated levels due to these stable atmospheric conditions, combined with the use of fireworks
 321 and firecrackers. In particular, some hours at the Danube site have been invalidated due to the negative chlorine
 322 levels attributed to these particular sources, which emit chlorinated species that may be poorly and/or slowly
 323 vaporized and not accounted for in the fragmentation table (such as chlorates, perchlorates) (Schmid et al., 2014).

324



325





327 **Figure 3: PM₁ species at the Danube (top) and Clemenceau (bottom) sites during the studied period.**

328 The average mass concentrations of NR-PM₁ species and eBC presented in Table 1 showed only slight differences
 329 between the two sites, with overall higher levels at the Clemenceau site. This could be attributed to the proximity
 330 of primary exhaust and non-exhaust emissions from road traffic as well as more intense condensation and
 331 coagulation processes. It should also be noted that the environment of the Clemenceau station is more urbanized
 332 (city center) compared to the Danube site, which may also partly explain these observations. OA is associated
 333 with the highest concentrations at both sites - with values of 3.89 $\mu\text{g m}^{-3}$ and 4.3 $\mu\text{g m}^{-3}$ at the Danube and
 334 Clemenceau sites, respectively - reinforcing the interest in the apportionment of its main sources. The second
 335 main compound at both sites was nitrate, with concentrations about 3020% higher at Clemenceau compared to
 336 Danube. As for OA, the difference The differences in sulfate and eBC_{ff} concentrations is are about 15 % on average
 337 (with the highest concentrations still observed at Clemenceau). Complementarily, results from offline analyses
 338 performed on filters collected in February 2020 indicate slightly higher concentrations for Clemenceau (Table 1).
 339 Surprisingly, however, filter-based levoglucosan analyses indicate similar concentration levels at both sites while
 340 eBC_{wb} appears to be about 40 % higher at Clemenceau, and the comparison of OA mass spectra averaged over
 341 the study period also indicates significantly higher signals for the highest m/z's, including common wood-burning
 342 tracers (see Figure S3), at Clemenceau.

343 **Table 1. Average (\pm standard deviation) mass concentrations of PM₁ species (in $\mu\text{g m}^{-3}$) at both Strasbourg sites during**
 344 **the studied period.**

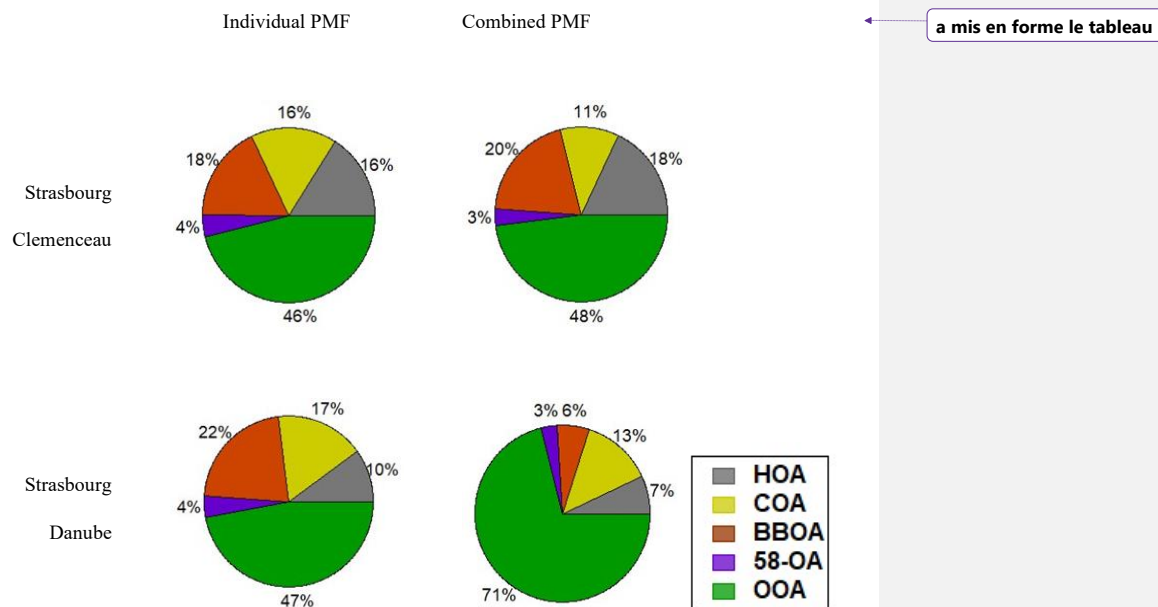
Species	Danube	Clem.	Danube	Clem.	Danube	Clem.
	ACSM/AE33 (DJF)		Filters (4-29 Feb.)		ACSM/AE33 (4-29 Feb.)	
OA	3.89 \pm 3.6	4.3 \pm 4.0			2.5 \pm 3.1	3.2 \pm 4.0
SO ₄	0.6 \pm 0.7	0.7 \pm 0.8	0.4 \pm 0.3	0.4 \pm 0.3	0.3 \pm 0.5	0.45 \pm 0.6
NO ₃	1.78 \pm 2.1	2.3 \pm 2.5	0.7 \pm 1.2	0.8 \pm 1.4	0.9 \pm 1.5	1.3 \pm 2.1
NH ₄	0.7 \pm 0.8	0.9 \pm 0.9	0.3 \pm 0.5	0.3 \pm 0.5	0.4 \pm 0.6	0.5 \pm 0.8
eBC _{ff}	0.75 \pm 0.7	0.8 \pm 0.9			0.6 \pm 0.7	0.7 \pm 1.2
eBC _{wb}	0.3 \pm 0.3	0.5 \pm 0.5			0.2 \pm 0.3	0.3 \pm 0.5
EC			0.7 \pm 0.5	0.9 \pm 0.7		
OC			2.0 \pm 1.7	2.2 \pm 2.0		
Levo.			0.13 \pm 0.13	0.13 \pm 0.14		

a mis en forme le tableau

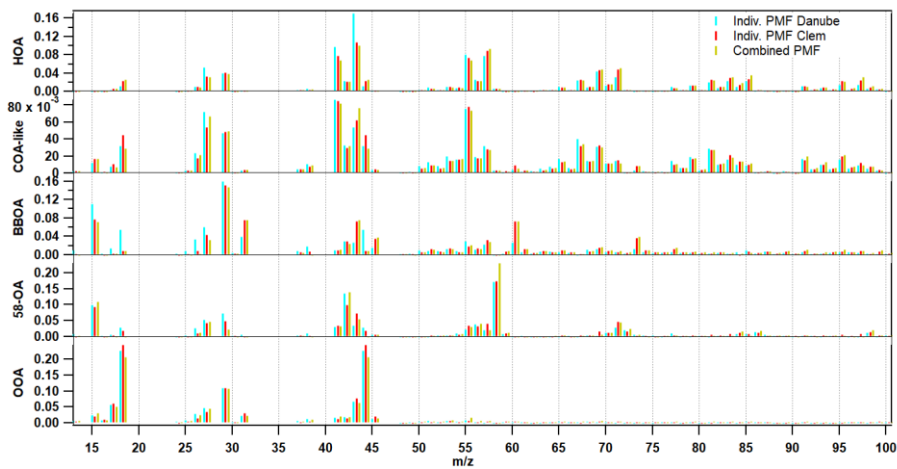
346 **4 OA source apportionment**

347 Figures 4 and 5 summarize the results of the individual and combined PMF analyses for the two sites, respectively,
348 showing the relative contributions of each identified OA factor and their corresponding mass spectra. These results
349 are described in the following paragraphs, according to their nature.

350



351 Figure 4: Contributions of OA factors at both sites from individual and combined PMF.



352

353 Figure 5: Mass spectra of OA factors from individual and combined PMF for both sites.

354 **4.1 Amine-related OA**

355 A noticeable result of the present study is the identification of a specific amine-related OA factor that was observed
 356 at both sites. This unusual factor is characterized by a high proportion of m/z 58 (mainly C₃H₈N⁺), with a
 357 contribution of about 4 % of the total OA mass. It was observed in both unconstrained and constrained PMF
 358 analyses and regardless of the number of factors or specific runs, the unconstrained PMF consistently revealed
 359 this factor among the 4-factor (or more) solutions. It showed a relatively stable profile across different PMF runs
 360 with high contributions from m/z 58 and 42 (C₂H₄N⁺). The time series for this factor at both sites show a highly
 361 variable temporal pattern with rather sporadic and intense peaks. The diel profile for this factor is not fully flat,
 362 displaying a slight peak in the morning and increasing towards the end of the day. However, associating this diel
 363 profile with a specific source proved to be challenging. Numerous tests were carried out in other seasons for
 364 continued measurements performed at the Danube site after the winter campaign presented in this paper. The 58-
 365 OA factor also emerged during a single study conducted in the summer, suggesting that it is not exclusively
 366 associated with winter sources.

367 The average mass spectrum for this factor differs from the few m/z 58-rich factors observed in previous studies
 368 based on AMS or ACSM measurements (Hildebrandt et al., 2011; Chen et al., 2021), where this factor was more
 369 likely associated with an instrument artifact. In particular, we observe high peaks for m/z 58 and 42, rather than
 370 the higher masses (m/z 84 and 98) observed in these previous studies. Furthermore, this factor does not appear
 371 when analyzing the Metz (pre-campaign) data with the same two instruments. This suggests that the factor is more
 372 closely related to local sources in Strasbourg.

373 The pollution rose analysis at both Strasbourg sites shows a specific and localized direction associated with this
 374 amine-related OA factor (Figure S16S18). The direction indicated an industrial area that could explain these
 375 specific particle emissions. A factor profile associated with amine-OA and a specific daily profile are consistent
 376 with an industrial source. This factor could therefore be associated with an industrial source of OA. Upon
 377 examining the emission inventory, we found a significant amount of particulate emissions linked to an industry
 378 zone, which aligns with the pollution roses. Although we found almost no info on the processes used in that type
 379 of industry, it seems polyamines are used in the production process of asphalt production as an example (as
 380 indicated in the Chinese patent, <https://patents.google.com/patent/CN102604125B/en>).

381 **4.2 Other POA factors**

382 Besides this site-specific amine-related factor, the PMF analyses identified the three main POA factors commonly
 383 observed in such a source apportionment analysis at urban sites, namely HOA, BBOA, and a COA-like factor.
 384 For HOA, the mass spectrum fingerprint is characterized by a high contribution of hydrocarbon fragments m/z
 385 41, 43, 55, 57, 69, and 71, and its time series shows well-defined diel variations associated with morning and
 386 evening traffic peaks corresponding to home/work commutes. The BBOA factor is characterized by a high
 387 contribution at m/z 29, 60, and 73 (tracers of biomass combustion) and by a diel variation showing an increase in
 388 the evening that extends into the night, associated with residential heating in winter. Some differences were
 389 observed between the BBOA profiles at the two sites. These differences can be explained by particle aging,
 390 especially with a higher 44/60 ratio at the Danube site than at the Clemenceau site, indicating more oxidized
 391 particles from biomass burning at the Danube site. Compared to HOA and BBOA, COA profiles are usually
 392 characterized by higher peaks at m/z 41 and 55, and by diel cycles showing midday (lunch) and evening (dinner)
 393 peaks associated with cooking activities. Such a clear diel profile could not be obtained for the Danube site, where
 394 it shows variations quite similar to those of BBOA, with a concentration maximum in the late evening. Therefore,
 395 we rather refer to this factor as COA-like.

396 For individual PMF outputs, HOA, BBOA, and COA-like contributed 16 %, 16 %, and 18 % of the organic matter,
 397 respectively, at the Clemenceau site. A lower HOA contribution (10 %) was observed for Danube, consistent with
 398 an increased influence of traffic at the Clemenceau site. The two primary factors HOA and BBOA showed a strong
 399 correlation with eBC_{fr} and eBC_{wb} (r^2 (HOA, eBC_{fr}) = 0.81 and 0.73; and r^2 (BBOA, eBC_{wb}) = 0.92 and 0.90 for
 400 the Clemenceau and Danube sites, respectively, Figure S13S15, SI). COA-like at the Danube site has a fairly
 401 similar contribution to COA-like at the Clemenceau site (about 17 %) but with a lower mass concentration of 0.6
 402 $\mu\text{g m}^{-3}$ compared to Clemenceau (0.9 $\mu\text{g m}^{-3}$) which is closer to the city center. However, BBOA shows a higher
 403 contribution at the Danube site (22 % of the total OA mass) with a concentration of 0.8 $\mu\text{g m}^{-3}$, close to that of
 404 Clemenceau which could be explained by the differences in the factor profile. A in comparison of m/z 60 at
 405 Danube and Clemenceau (Figure S14S16 in the SI) shows an m/z 60 signal twice as high at Clemenceau as at
 406 Danube.

407 The results of the combined PMF analysis may help to gain a deeper understanding of the variation of these POA
408 factors between the two sites. Interestingly, the contributions obtained from the combined PMF differ from those
409 obtained using the individual PMF for Danube, whereas only minor differences are obtained for Clemenceau, with
410 slightly more HOA and BBOA and less COA-like at this site (Figure 5). For the Danube site, however, the relative
411 contributions and mass concentrations of these factors are significantly altered, especially for HOA and BBOA.
412 The COA-like factor shows similar mass concentrations close to $0.6 \mu\text{g m}^{-3}$, representing 17 % and 13 % of the
413 total mass for the individual and combined PMF, respectively. HOA also decreased slightly from 10 % to 7 %
414 between the two PMF approaches. A strong decrease in BBOA is observed, from 22 % to 6 %, consistent with
415 the m/z 60 comparison showing less fresh BBOA at the Danube site. In fact, the BBOA profile for the combined
416 PMF is more similar to the BBOA profile for the individual PMF at the Clemenceau site compared to the Danube
417 site.

418 **4.3 Oxygenated organic aerosols (OOA)**

419 The obtained OOA mass spectra are consistent with those reported in the literature, associated with a stable diel
420 variation, and characterized by a high contribution of m/z 44 (Figure S10S12). At both sites, the OOA factor
421 showed similar profiles and diel variations. For the individual PMF, OOA dominated OA at both sites with a
422 contribution of about 47 % but with different mass concentrations of 2.6 and $1.7 \mu\text{g m}^{-3}$ at the Clemenceau and
423 Danube sites, respectively.

424 The combined PMF identified two OOA factors, named OOA1 and OOA2 (section S2, Figure S9S11). Because
425 the two factors are correlated, we summed them together to obtain a single OOA factor (Figure S11S13). At the
426 Clemenceau site, the contribution of the OOA factor (48 %) is similar to the one obtained from the individual
427 PMF, with a mass concentration of $2.8 \mu\text{g m}^{-3}$. At the Danube site, the contribution of the OOA factor strongly
428 increased from 47 % for the individual PMF to 71 % for the combined one (Figure 4), reaching a mass
429 concentration of $2.6 \mu\text{g m}^{-3}$, close to that of the Clemenceau site. These combined PMF results provided further
430 insight into this factor and demonstrated its regional origin. In Clemenceau, we observed a balance between
431 primary and secondary OA factors, while for Danube, the combined PMF results indicated an average OOA
432 contribution of about 70 % of the total OA.

433

434 **5 Discussion and concluding remarks**

435 The present study provides an opportunity to qualitatively assess the measurement consistency and results of
436 carbonaceous aerosol source apportionment analyses conducted with the same type of instrument at two
437 neighboring urban sites. The two ACSMs used in this study to characterize non-refractory submicron chemical
438 species were first compared at the same location prior to the campaign. This side-by-side comparison showed a
439 very good agreement for nitrate concentrations, confirming the consistency of the response factors obtained from
440 the calibration of both ACSMs. However, significant discrepancies - of about 30 % - were obtained for OA (and
441 sulfate) mass concentrations, and the comparison of OA mass spectra showed a surprising behavior with a few
442 m/z 's (including m/z 60 and 73, commonly used as biomass burning tracers) at higher levels in the instrument
443 which presented overall lower loadings in total OA concentrations. Quality assurance and quality checks were
444 performed according to the most advanced recommendations provided by the manufacturer and the scientific
445 community, and no specific instrumental bias could be identified to explain these differences. Therefore, both
446 ACSMs can be considered as running under their usual and proper operating conditions, with discrepancies mainly
447 due to inherent technical specificities of each instrument. It should be noted that the two ACSMs do not have the
448 same age or date of manufacture (the Clemenceau ACSM dates from 2014 and the Danube ACSM from 2018),
449 which may influence the evolution of the instrument over time.

450 Once installed at their respective monitoring stations in Strasbourg, the ACSMs provided meaningful
451 measurements of the submicron aerosol chemical species, with moderately higher concentrations at the
452 Clemenceau traffic site compared to the urban background Danube station, which can be attributed to more intense
453 primary emissions and/or transformation processes at the roadside. Filter-based offline measurements available
454 for the last month of the campaign tend to confirm these observations, with slightly higher concentrations of major
455 chemical species at Clemenceau. Results from individual PMF analyses also indicated higher HOA contributions
456 for Clemenceau, in good agreement with moderately higher eBC_{ff} and EC concentrations at the same site
457 compared to Danube. They also pointed to similar BBOA contributions at the two stations, in agreement with the
458 comparison of filter-based levoglucosan measurements. Less expected is the significantly higher eBC_{wb} loading

459 obtained from the application of the so-called Aethalometer model to AE33 measurements at both sites. This may
460 be due to the choice of site-specific sets of AAE values (α_{ff} and α_{wb}) chosen to represent the two eBC subfractions
461 at each monitoring site. This result confirms the high sensitivity of the Aethalometer model to the empirical
462 assumptions to be made for its application. In particular, this may illustrate how cautiously it should be considered
463 for any eBC source apportionment study at a traffic site (e.g., Savadkoohi et al., 2023).

464 The COA-like factor showed the expected peaks at lunch and dinner time for Clemenceau, but also a diel cycle
465 relatively similar to BBOA (with no significant midday increase) for Danube, illustrating the difficulty in
466 attributing a pure cooking origin to this factor. Interestingly, the results of the combined PMF analysis may
467 improve the apportionment of these cooking emissions, reducing the COA-to-HOA ratio at night - especially for
468 Clemenceau - compared to individual PMF outputs (Fig. S12S14). However, such a combined PMF analysis may
469 not be suitable to improve the consistency of other OA factors, probably due to instrumental specificities leading
470 to differences in the OA mass spectra obtained by the two instruments. More specifically, the OA profiles obtained
471 by the combined PMF method exhibit a greater similarity to the profiles obtained by the individual PMF analysis
472 at Clemenceau than to those obtained by the individual PMF analysis at Danube. As a result, there is a reduced
473 contribution of m/z 43 (associated with HOA) and m/z 44 (associated with BBOA) at Danube when applying the
474 combined PMF approach as opposed to the individual PMF analyses. This discrepancy leads to an underestimation
475 of these factors (HOA and BBOA) and an overestimation of OOA at the Danube site when using the combined
476 PMF method.

477 Finally, simultaneous ACSM measurements at these paired sites allow to confirm the existence and substantial
478 influence of an amine-related OA factor in Strasbourg. This unique factor, characterized by a high proportion of
479 m/z 58, represents approximately 4 % of the total OA mass and is consistently observed in both PMF analyses.
480 The diel profile of this factor shows peaks in the morning and late in the day, but its specific source remains
481 challenging to identify. It differs from previously observed m/z 58-rich factors, suggesting a distinct local source,
482 possibly related to industrial emissions. Further investigation is needed to determine the exact source of this
483 intriguing amine-related OA factor.

484 In summary, the comparison of different PMF methods carried out in this study highlights caveats and limitations
485 inherent to such kind of SA approach. First, the elucidation of OA sources based on factors derived from PMF
486 should be interpreted with caution considering real-world . In addition, attention should be exercised when
487 combining data from different measurement instruments, as they are not strictly identical in terms of sensitivity.
488 However, positioning two instruments in the same location (or close to each other) can help to verify the presence
489 of atypical or unique factors and explain discrepancies. These limitations introduce uncertainties in the
490 apportionment of OA sources and in the consistency of factor interpretation. In order to improve the identification
491 and interpretation of PMF factors, we propose the integration of complementary datasets (e.g., molecular tracers),
492 which would provide additional constraints. Future work should include a focus on refined methodologies to better
493 handle multi-instrument and multi-timescale datasets, and on the elaboration of standardized protocols for inter-
494 instrument comparisons. Ultimately, improving these methods will lead to a better understanding of the sources,
495 evolution, and role of OA in the atmosphere, which is crucial for accurately assessing their impacts on air quality,
496 health, and climate.

497

498 Data availability

499 Data for Strasbourg Danube are available at <https://doi.org/10.5281/zenodo.13318298> (Chebaicheb et al., 2024).
500 Data for Strasbourg Clemenceau are available at <https://doi.org/10.5281/zenodo.14855186> (Chebaicheb et al.,
501 2025). More details on the analyses are available upon request to the contact author Hasna Chebaicheb
502 (hasna.chebaicheb@ineris.fr).

Code de champ modifié

Code de champ modifié

503 Author contributions

504 HC: Data curation, Formal analysis, Investigation, Methodology, Visualisation, Conceptualization, Writing -
505 Original Draft

506 MC: Data curation, Formal analysis, Visualisation, Conceptualization, Resources, Writing - Original Draft

507 OF: Conceptualization, Methodology, Validation, Supervision, Writing - Original Draft, Project administration,
508 Funding acquisition
509 JB: Conceptualization, Validation, Supervision, Writing - Review & Editing
510 VC: Conceptualization, Writing - Review & Editing
511 TA: Conceptualization, Writing - Review & Editing
512 MG: Formal analysis, Writing - Review & Editing
513 EJ: Conceptualization, Writing - Review & Editing
514 CM: Conceptualization, Supervision, Writing - Review & Editing
515 VR: Conceptualization, Validation, Supervision, Writing - Review & Editing, Project administration, Funding
516 acquisition

517 **Acknowledgments**

518 IMT Nord Europe and INERIS participated in the COST COLOSSAL Action CA16109.

519 **Funding**

520 H. Chebaicheb's PhD grant was supported by the LCSQA funded by the French Ministry of Environment. IMT
521 Nord Europe also acknowledges financial support from the Labex CaPPA project, which is funded by the French
522 National Research Agency (ANR) through the PIA (Programme d'Investissement d'Avenir) under contract ANR-
523 11-LABX-0005-01.

524 **Conflicts of Interest.** The authors declare no conflict of interest.

525 **References**

526 Äijälä, M., Heikkinen, L., Fröhlich, R., Canonaco, F., Prévôt, A. S. H., Junninen, H., Petäjä, T., Kulmala, M.,
527 Worsnop, D., and Ehn, M.: Resolving anthropogenic aerosol pollution types – deconvolution and exploratory
528 classification of pollution events, *Atmospheric Chem. Phys.*, 17, 3165–3197, <https://doi.org/10.5194/acp-17-3165-2017>, 2017.

530 Aiken, A.C., DeCarlo, P.F., Kroll, J.H., Worsnop, D.R., Huffman, J.A., Docherty, K.S., Ulbrich, I.M., Mohr, C.,
531 Kimmel, J.R., Sueper, D., Sun, Y., Zhang, Q., Trimborn, A., Northway, M., Ziemann, P.J., Canagaratna, M.R.,
532 Onasch, T.B., Alfarra, M.R., Prevot, A.S.H., Dommen, J., Duplissy, J., Metzger, A., Baltensperger, U., Jimenez,
533 J.L., 2008. O/C and OM/OC Ratios of Primary, Secondary, and Ambient Organic Aerosols with High-Resolution
534 Time-of-Flight Aerosol Mass Spectrometry. *Environ. Sci. Technol.* 42, 4478–4485.
535 <https://doi.org/10.1021/es703009q>.

536 Air quality in Europe 2022 — European Environment Agency: <https://www.eea.europa.eu/publications/air-quality-in-europe-2022>, last access: 31 July 2023.

538 ATMO Grand Est: Le bilan annuel 2022 de la qualité de l'air dans le Grand Est, <https://www.atmograndest.eu/actualite/le-bilan-annuel-2022-de-la-qualite-de-lair-dans-le-grand-est>, last access: 31 July 2023.

540 Bressi, M., Cavallii, F., Putaud, J.P., Fröhlich, R., Petit, J.-E., Aas, W., Äijälä, M., Alastuey, A., Allan, J.D., Aurela,
541 M., Berico, M., Bougiatioti, A., Bukowiecki, N., Canonaco, F., Crenn, V., Dusanter, S., Ehn, M., Elsasser, M.,
542 Flentje, H., Graf, P., Green, D.C., Heikkinen, L., Hermann, H., Holzinger, R., Hueglin, C., Keernik, H., Kiendler-
543 Scharr, A., Kubelová, L., Lunder, C., Maasikmets, M., Makeš, O., Malagutti, A., Mihalopoulos, N., Nicolas, J.B.,
544 O'Dowd, C., Ovadnevaite, J., Petralia, E., Poulain, L., Priestman, M., Riffault, V., Ripoll, A., Schlag, P., Schwarz,
545 J., Sciare, J., Slowik, J., Sosedova, Y., Stavroulas, I., Teinemaa, E., Via, M., Vodička, P., Williams, P.I.,

546 Wiedensohler, A., Young, D.E., Zhang, S., Favez, O., Minguillón, M.C., Prevot, A.S.H., 2021. A European
547 aerosol phenomenology - 7: High-time resolution chemical characteristics of submicron particulate matter across
548 Europe. *Atmospheric Environment*: X 10, 100108. <https://doi.org/10.1016/j.aeaoa.2021.100108>.

Code de champ modifié

549 Cavalli, F., Viana, M., Yttri, K.E., Genberg, J., Putaud, J.-P., 2010. Toward a standardised thermal-optical protocol
550 for measuring atmospheric organic and elemental carbon: the EUSAAR protocol. *Atmospheric Measurement
551 Techniques* 3, 79–89. <https://doi.org/10.5194/amt-3-79-2010>.

552 Chatain, M., Alvarez, R., Ustache, A., Rivière, E., Favez, O., and Pallares, C.: Simultaneous Roadside and Urban
553 Background Measurements of Submicron Aerosol Number Concentration and Size Distribution (in the Range 20–
554 800 nm), along with Chemical Composition in Strasbourg, France, *Atmosphere*, 12, 71,
555 <https://doi.org/10.3390/atmos12010071>, 2021.

556 Chebaicheb, H., F. de Brito, J., Chen, G., Tison, E., Marchand, C., Prévôt, A. S. H., Favez, O., and Riffault, V.:
557 Investigation of four-year chemical composition and organic aerosol sources of submicron particles at the ATOLL
558 site in northern France, *Environ. Pollut.*, 330, 121805, <https://doi.org/10.1016/j.envpol.2023.121805>, 2023.

559 Chebaicheb, H., de Brito, J. F., Amodeo, T., Couvidat, F., Petit, J.-E., Tison, E., Abbou, G., Baudic, A., Chatain,
560 M., Chazeau, B., Marchand, N., Falhun, R., Francony, F., Ratier, C., Grenier, D., Vidaud, R., Zhang, S., Gille, G.,
561 Meunier, L., Marchand, C., Riffault, V., and Favez, O.: Multiyear high-temporal-resolution measurements of
562 submicron aerosols at 13 French urban sites: data processing and chemical composition, *Earth Syst. Sci. Data*, 16,
563 5089–5109, <https://doi.org/10.5194/essd-16-5089-2024>, 2024.

564 Chebaicheb, H., Ferreira de Brito, J., Amodeo, T., Couvidat, F., Petit, J.-E., Tison, E., Abbou, G., Alexia, B.,
565 Chatain, M., Chazeau, B., Marchand, N., Falhun, R., Francony, F., Ratier, C., Grenier, D., Vidaud, R., Zhang, S.,
566 Gille, G., Meunier, L., Marchand, C., Riffault, V., and Favez, O.: Multi-year high time resolution measurements
567 of fine PM at 13 sites of the French Operational Network (CARA program), In *Earth System Science Data*, Zenodo
568 [data set], <https://doi.org/10.5281/zenodo.13318298>, 2024.

Code de champ modifié

569 Chebaicheb, H., Chatain, M., Favez, O., Ferreira de Brito, J., Crenn, V., Amodeo, T., Gherras, M., Jantzem, E.,
570 Marchand, C., & Riffault, V. (2025). Lessons learned from the comparison and combination of fine carbonaceous
571 aerosol source apportionment at two locations in the city of Strasbourg, France [Data set]. In *Atmospheric
572 Chemistry and Physics (ACP)*. Zenodo. <https://doi.org/10.5281/zenodo.14855186>.

Code de champ modifié

573 Chen, G., Sosedova, Y., Canonaco, F., Fröhlich, R., Tobler, A., Vlachou, A., Daellenbach, K. R., Bozzetti, C.,
574 Hueglin, C., Graf, P., Baltensperger, U., Slowik, J. G., El Haddad, I., and Prévôt, A. S. H.: Time-dependent source
575 apportionment of submicron organic aerosol for a rural site in an alpine valley using a rolling positive matrix
576 factorization (PMF) window, *Atmospheric Chem. Phys.*, 21, 15081–15101, <https://doi.org/10.5194/acp-21-15081-2021>, 2021.

577 Chen, G., Canonaco, F., Tobler, A., Aas, W., Alastuey, A., Allan, J., Atabakhsh, S., Aurela, M., Baltensperger,
578 U., Bougiatioti, A., De Brito, J. F., Ceburnis, D., Chazeau, B., Chebaicheb, H., Daellenbach, K. R., Ehn, M., El
579 Haddad, I., Eleftheriadis, K., Favez, O., Flentje, H., Font, A., Fossum, K., Freney, E., Gini, M., Green, D. C.,
580 Heikkinen, L., Herrmann, H., Kalogridis, A.-C., Keernik, H., Lhotka, R., Lin, C., Lunder, C., Maasikmets, M.,
581 Manousakas, M. I., Marchand, N., Marin, C., Marmureanu, L., Mihalopoulos, N., Močnik, G., Nęcki, J., O'Dowd,
582 C., Ovadnevaite, J., Peter, T., Petit, J.-E., Pikridas, M., Matthew Platt, S., Pokorná, P., Poulain, L., Priestman, M.,
583 Riffault, V., Rinaldi, M., Różański, K., Schwarz, J., Sciare, J., Simon, L., Skiba, A., Slowik, J. G., Sosedova, Y.,
584 Stavroulas, I., Styszko, K., Teinemaa, E., Timonen, H., Tremper, A., Vasilescu, J., Via, M., Vodička, P.,
585 Wiedensohler, A., Zografas, O., Cruz Minguillón, M., and Prévôt, A. S. H.: European aerosol phenomenology –
586 8: Harmonised source apportionment of organic aerosol using 22 Year-long ACSM/AMS datasets, *Environ. Int.*,
587 166, 107325, <https://doi.org/10.1016/j.envint.2022.107325>, 2022.

588 Crippa, M., DeCarlo, P. F., Slowik, J. G., Mohr, C., Heringa, M. F., Chirico, R., Poulain, L., Freutel, F., Sciare,
589 J., Cozic, J., Di Marco, C. F., Elsasser, M., Nicolas, J. B., Marchand, N., Abidi, E., Wiedensohler, A., Drewnick,
590 F., Schneider, J., Borrmann, S., Nemitz, E., Zimmermann, R., Jaffrezo, J.-L., Prévôt, A. S. H., and Baltensperger,
591 U.: Wintertime aerosol chemical composition and source apportionment of the organic fraction in the metropolitan
592 area of Paris, *Atmospheric Chem. Phys.*, 13, 961–981, <https://doi.org/10.5194/acp-13-961-2013>, 2013.

594 Drinovec, L., Močnik, G., Zotter, P., Prévôt, A. S. H., Ruckstuhl, C., Coz, E., Rupakheti, M., Sciare, J., Müller,
 595 T., Wiedensohler, A., and Hansen, A. D. A.: The “dual-spot” Aethalometer: an improved measurement of aerosol
 596 black carbon with real-time loading compensation, *Atmospheric Meas. Tech.*, 8, 1965–1979,
 597 <https://doi.org/10.5194/amt-8-1965-2015>, 2015.

598 Favez, O., Weber, S., Petit, J.-E., Alleman, L., Albinet, A., Riffault, V., Chazeau, B., Amodeo, T., Salameh, D.,
 599 Zhang, Y., Srivastava, D., Samaké, A., Aujay, R., Papin, A., Bonnaire, N., Boullanger, C., Chatain, M., Chevrier,
 600 F., Detournay, A., and Leoz-Garziandia, E.: Overview of the French Operational Network for In Situ Observation
 601 of PM Chemical Composition and Sources in Urban Environments (CARA Program),
 602 <https://doi.org/10.20944/preprints202101.0182.v1>, 2021.

603 Guide méthodologique pour la mesure des concentrations en ammoniac dans l'air ambiant | LCSQA:
 604 <https://www.lcsqa.org/fr/rapport/guide-methodologique-pour-la-mesure-des-concentrations-en-ammoniac-dans->
 605 air-ambiant, last access: 31 July 2023.

606 Hildebrandt, L., Kostendou, E., Lanz, V. A., Prevot, A. S. H., Baltensperger, U., Mihalopoulos, N., Laaksonen,
 607 A., Donahue, N. M., and Pandis, S. N.: Sources and atmospheric processing of organic aerosol in the
 608 Mediterranean: insights from aerosol mass spectrometer factor analysis, *Atmospheric Chem. Phys.*, 11, 12499–
 609 12515, <https://doi.org/10.5194/acp-11-12499-2011>, 2011.

610 Hopke, P. K., Dai, Q., Li, L., and Feng, Y.: Global review of recent source apportionments for airborne particulate
 611 matter, *Sci. Total Environ.*, 740, 140091, <https://doi.org/10.1016/j.scitotenv.2020.140091>, 2020.

612 Katz, E. F., Guo, H., Campuzano-Jost, P., Day, D. A., Brown, W. L., Boedicker, E., Pothier, M., Lunderberg, D.
 613 M., Patel, S., Patel, K., Hayes, P. L., Avery, A., Hildebrandt Ruiz, L., Goldstein, A. H., Vance, M. E., Farmer, D.
 614 K., Jimenez, J. L., and DeCarlo, P. F.: Quantification of cooking organic aerosol in the indoor environment using
 615 aerodyne aerosol mass spectrometers, *Aerosol Science and Technology*, 55, 1099–1114,
 616 <https://doi.org/10.1080/02786826.2021.1931013>, 2021.

617 Kim, B.M., Cassmassi, J., Hogo, H., Zeldin, M.D., 2001. Positive Organic Carbon Artifacts on Filter Medium
 618 During PM_{2.5} Sampling in the South Coast Air Basin. *Aerosol Science and Technology* 34, 35–41.
 619 <https://doi.org/10.1080/02786820118227>.

620 Laj, P., Myhre, C.L., Riffault, V., Amiridis, V., Fuchs, H., Eleftheriadis, K., Petäjä, T., Salameh, T., Kivekäs, N.,
 621 Juurula, E., Saponaro, G., Philippin, S., Cornacchia, C., Arboledas, L.A., Baars, H., Claude, A., Mazière, M.D.,
 622 Dils, B., Dufresne, M., Evangelou, N., Favez, O., Fiebig, M., Haeffelin, M., Herrmann, H., Höhler, K., Illmann,
 623 N., Kreuter, A., Ludewig, E., Marinou, E., Möhler, O., Mona, L., Murberg, L.E., Nicolae, D., Novelli, A.,
 624 O'Connor, E., Ohneiser, K., Altieri, R.M.P., Picquet-Varrault, B., Pinxteren, D. van, Pospichal, B., Putaud, J.-P.,
 625 Reimann, S., Siomos, N., Stachiewska, I., Tillmann, R., Voudouri, K.A., Wandering, U., Wiedensohler, A.,
 626 Apituley, A., Comerón, A., Gysel-Beer, M., Mihalopoulos, N., Nikolova, N., Pietruczuk, A., Sauvage, S., Sciare,
 627 J., Skov, H., Svendby, T., Swietlicki, E., Tonev, D., Vaughan, G., Zdimal, V., Baltensperger, U., Doussin, J.-F.,
 628 Kulmala, M., Pappalardo, G., Sundet, S.S., Vana, M., 2024. Aerosol, Clouds and Trace Gases Research
 629 Infrastructure (ACTRIS): The European Research Infrastructure Supporting Atmospheric Science. *Bulletin of the*
 630 *American Meteorological Society* 105, E1098–E1136. <https://doi.org/10.1175/BAMS-D-23-0064.1>.

631 Li, S., Chen, C., Yang, G., Fang, J., Sun, Y., Tang, L., Wang, H., Xiang, W., Zhang, H., Croteau, P.L., Jayne, J.T.,
 632 Liao, H., Ge, X., Favez, O., Zhang, Y., 2022. Sources and processes of organic aerosol in non-refractory PM₁ and
 633 PM_{2.5} during foggy and haze episodes in an urban environment of the Yangtze River Delta, China. *Environmental*
 634 *Research* 212, 113557. <https://doi.org/10.1016/j.envres.2022.113557>.

635 Liu, P.S.K., Deng, R., Smith, K.A., Williams, L.R., Jayne, J.T., Canagaratna, M.R., Moore, K., Onasch, T.B.,
 636 Worsnop, D.R., Deshler, T., 2007. Transmission Efficiency of an Aerodynamic Focusing Lens System:
 637 Comparison of Model Calculations and Laboratory Measurements for the Aerodyne Aerosol Mass Spectrometer.
 638 *Aerosol Science and Technology* 41, 721–733. <https://doi.org/10.1080/02786820701422278>.

639 Masson-Delmotte, V., Zhai, P., Pirani, A., Connors, S. L., Péan, C., Berger, S., Caud, N., Chen, Y., Goldfarb, L.,
 640 Gomis, M. I., Huang, M., Leitzell, K., Lonnoy, E., Matthews, J. B. R., Maycock, T. K., Waterfield, T., Yelekçi,
 641 Ö., Yu, R., and Zhou, B. (Eds.): *Climate Change 2021: The Physical Science Basis. Contribution of Working*

Code de champ modifié

Code de champ modifié

642 Group I to the Sixth Assessment Report of the Intergovernmental Panel on Climate Change, Cambridge University
 643 Press, Cambridge, United Kingdom and New York, NY, USA, <https://doi.org/10.1017/9781009157896>, 2021.

644 Middlebrook, A.M., Bahreini, R., Jimenez, J.L., Canagaratna, M.R., 2011. Evaluation of Composition-Dependent
 645 Collection Efficiencies for the Aerodyne Aerosol Mass Spectrometer using Field Data. *Aerosol Science and*
 646 *Technology* 46, 258–271. <https://doi.org/10.1080/02786826.2011.620041>.

647 Mooibroek, D., Schaap, M., Weijers, E. P., and Hoogerbrugge, R.: Source apportionment and spatial variability
 648 of PM_{2.5} using measurements at five sites in the Netherlands, *Atmos. Environ.*, 45, 4180–4191,
 649 <https://doi.org/10.1016/j.atmosenv.2011.05.017>, 2011.

650 Mooibroek, D., Staelens, J., Cordell, R., Panteliadis, P., Delaunay, T., Weijers, E., Vercauteren, J., Hoogerbrugge,
 651 R., Dijkema, M., Monks, P. S., and Roekens, E.: PM₁₀ Source Apportionment in Five North Western European
 652 Cities—Outcome of the Joaquin Project, <https://doi.org/10.1039/9781782626589-00264>, 2016.

653 Nault, B. A., Croteau, P., Jayne, J., Williams, A., Williams, L., Worsnop, D., Katz, E. F., DeCarlo, P. F., and
 654 Canagaratna, M.: Laboratory evaluation of organic aerosol relative ionization efficiencies in the aerodyne aerosol
 655 mass spectrometer and aerosol chemical speciation monitor, *Aerosol Science and Technology*, 57, 981–997,
 656 <https://doi.org/10.1080/02786826.2023.2223249>, 2023.

657 Ng, N. L., Herndon, S. C., Trimborn, A., Canagaratna, M. R., Croteau, P. L., Onasch, T. B., Sueper, D., Worsnop,
 658 D. R., Zhang, Q., Sun, Y. L., and Jayne, J. T.: An Aerosol Chemical Speciation Monitor (ACSM) for Routine
 659 Monitoring of the Composition and Mass Concentrations of Ambient Aerosol, *Aerosol Sci. Technol.*, 45, 780–
 660 794, <https://doi.org/10.1080/02786826.2011.560211>, 2011.

661 Paatero, P., Tapper, U., 1994. Positive matrix factorization: a non-negative factor model with optimal utilization
 662 of error estimates of data values. *Environmetrics* 5, 111–126. <https://doi.org/10.1002/env.3170050203>.

663 Pandolfi, M., Mooibroek, D., Hopke, P., van Pinxteren, D., Querol, X., Herrmann, H., Alastuey, A., Favez, O.,
 664 Hüglin, C., Perdrix, E., Riffault, V., Sauvage, S., van der Swaluw, E., Tarasova, O., Colette, A., 2020. Long-range
 665 and local air pollution: what can we learn from chemical speciation of particulate matter at paired sites?
 666 *Atmospheric Chemistry and Physics* 20, 409–429. <https://doi.org/10.5194/acp-20-409-2020>.

667 Petit, J.-E., Favez, O., Sciare, J., Canonaco, F., Croteau, P., Močnik, G., Jayne, J., Worsnop, D., and Leoz-
 668 Garziandia, E.: Submicron aerosol source apportionment of wintertime pollution in Paris, France by double
 669 positive matrix factorization (PMF²) using an aerosol chemical speciation monitor (ACSM) and a multi-
 670 wavelength Aethalometer, *Atmospheric Chem. Phys.*, 14, 13773–13787, <https://doi.org/10.5194/acp-14-13773-2014>, 2014.

671 Petit, J.-E., Pallares, C., Favez, O., Alleman, L., Bonnaire, N., and Rivière, E.: Sources and Geographical Origins
 672 of PM₁₀ in Metz (France) Using Oxalate as a Marker of Secondary Organic Aerosols by Positive Matrix
 673 Factorization Analysis, *Atmosphere*, 10, 370, <https://doi.org/10.3390/atmos10070370>, 2019.

674 Potier, E., Waked, A., Bourin, A., Minvielle, F., Péré, J.C., Perdrix, E., Michoud, V., Riffault, V., Alleman, L.Y.,
 675 Sauvage, S., 2019. Characterizing the regional contribution to PM10 pollution over northern France using two
 676 complementary approaches: Chemistry transport and trajectory-based receptor models. *Atmospheric Research*
 677 223, 1–14. <https://doi.org/10.1016/j.atmosres.2019.03.002>

678 Qi, L., Bozzetti, C., Corbin, J. C., Daellenbach, K. R., El Haddad, I., Zhang, Q., Wang, J., Baltensperger, U.,
 679 Prévôt, A. S. H., Chen, M., Ge, X., and Slowik, J. G.: Source identification and characterization of organic nitrogen
 680 in atmospheric aerosols at a suburban site in China, *Sci. Total Environ.*, 818, 151800, 2022.
 681 <https://doi.org/10.1016/j.scitotenv.2021.151800>, 2022.

682 Sandradewi, J., Prevot, A., Weingartner, E., Schmidhauser, R., Gysel, M., and Baltensperger, U.: A study of wood
 683 burning and traffic aerosols in an Alpine valley using a multi-wavelength Aethalometer, *Atmos. Environ.*, 42,
 684 101–112, <https://doi.org/10.1016/j.atmosenv.2007.09.034>, 2008.

685 Savadkoohi, M., [et al.](#), Gherras, M., Favez, O., Petit, J.-E., Rovira, J., Chen, G. I., Via, M., Platt, S., Aurela, M.,
 686 Chazeau, B., de Brito, J. F., Riffault, V., Eleftheriadis, K., Flentje, H., Gysel-Beer, M., Hueglin, C., Rigler, M.,
 687

Code de champ modifié

a mis en forme : Interligne : Multiple 1,15 li

688 Gregorić, A., Ivančić, M., Keernik, H., Maasikmets, M., Liakakou, E., Stavroulas, I., Luoma, K., Marchand, N.,
689 Mihalopoulos, N., Petäjä, T., Prevot, A. S. H., Daellenbach, K. R., Vodička, P., Timonen, H., Tobler, A.,
690 Vasilescu, J., Dandocsi, A., Mbengue, S., Vratolis, S., Zografoiu, O., Chauvigné, A., Hopke, P. K., Querol, X.,
691 Alastuey, A., and Pandolfi, M.: Addressing the advantages and limitations of using Aethalometer data to
692 determine the optimal Absorptionabsorption Ångström Exponentexponents (AAEs) values for eBC source
693 apportionment, 2025, submitted to Atmospheric Environment International, 349, 121121,
694 [https://doi.org/10.1016/j.atmosenv.2025.121121, 2025](https://doi.org/10.1016/j.atmosenv.2025.121121).

695 Schmid, P., Bogdal, C., Wang, Z., Azara, V., Haag, R., and von Arx, U.: Releases of chlorobenzenes,
696 chlorophenols and dioxins during fireworks, Chemosphere, 114, 158–164,
697 [https://doi.org/10.1016/j.chemosphere.2014.03.088, 2014](https://doi.org/10.1016/j.chemosphere.2014.03.088).

700 Tobler, A.K., Skiba, A., Canonaco, F., Močnik, G., Rai, P., Chen, G., Bartyzel, J., Zimnoch, M., Styszko, K.,
701 Nęcki, J., Furger, M., Różański, K., Baltensperger, U., Slowik, J.G., Prevot, A.S.H., 2021. Characterization of
702 non-refractory (NR) PM₁ and source apportionment of organic aerosol in Kraków, Poland. Atmospheric
703 Chemistry and Physics 21, 14893–14906. <https://doi.org/10.5194/acp-21-14893-2021>.

704 Via, M., Minguillón, M.C., Reche, C., Querol, X., Alastuey, A., 2021. Increase in secondary organic aerosol in
705 an urban environment. Atmospheric Chemistry and Physics 21, 8323–8339. <https://doi.org/10.5194/acp-21-8323-2021>.

706 Waked, A., Bourin, A., Michoud, V., Perdrix, E., Alleman, L.Y., Sauvage, S., Delaunay, T., Vermeesch, S., Petit,
707 J.-E., Riffault, V., 2018. Investigation of the geographical origins of PM10 based on long, medium and short-
708 range air mass back-trajectories impacting Northern France during the period 2009–2013. Atmospheric
709 Environment 193, 143–152. <https://doi.org/10.1016/j.atmosenv.2018.08.015>

710 WHO Air Quality Guidelines: https://www.c40knowledgehub.org/s/article/WHO-Air-Quality-Guidelines?language=en_US, last access: 23 January 2023.

711 Xu, W., Lambe, A., Silva, P., Hu, W., Onasch, T., Williams, L., Croteau, P., Zhang, X., Renbaum-Wolff, L.,
712 Fortner, E., Jimenez, J. L., Jayne, J., Worsnop, D., and Canagaratna, M.: Laboratory evaluation of species-
713 dependent relative ionization efficiencies in the Aerodyne Aerosol Mass Spectrometer, Aerosol Sci. Technol., 52,
714 626–641, [https://doi.org/10.1080/02786826.2018.1439570, 2018](https://doi.org/10.1080/02786826.2018.1439570).

715 Zhang, S., Tison, E., Dusander, S., Beaugard, C., Gengembre, C., Augustin, P., Fourmentin, M., Delbarre, H.,
716 Riffault, V., 2021. Near real-time PM1 chemical composition measurements at a French urban background and
717 coastal site under industrial influence over more than a year: Temporal variability and assessment of sulfur-
718 containing emissions. Atmospheric Environment 244, 117960. <https://doi.org/10.1016/j.atmosenv.2020.117960>

719 Zhang, Y., Favez, O., Petit, J.-E., Canonaco, F., Truong, F., Bonnaire, N., Crenn, V., Amodeo, T., Prévôt, A. S.
720 H., Sciare, J., Gros, V., and Albinet, A.: Six-year source apportionment of submicron organic aerosols from near-
721 continuous highly time-resolved measurements at SIRTA (Paris area, France), Atmospheric Chem. Phys., 19,
722 14755–14776, [https://doi.org/10.5194/acp-19-14755-2019, 2019](https://doi.org/10.5194/acp-19-14755-2019).

723 Zhang, Y., Albinet, A., Petit, J.-E., Jacob, V., Chevrier, F., Gille, G., Pontet, S., Chrétien, E., Dominik-Sègue, M.,
724 Levigoureux, G., Močnik, G., Gros, V., Jaffrezo, J.-L., Favez, O., 2020. Substantial brown carbon emissions from
725 wintertime residential wood burning over France. Science of The Total Environment 743, 140752.
726 <https://doi.org/10.1016/j.scitotenv.2020.140752>.

727 Zhou, S., Collier, S., Xu, J., Mei, F., Wang, J., Lee, Y.-N., Sedlacek III, A. J., Springston, S. R., Sun, Y., and
728 Zhang, Q.: Influences of upwind emission sources and atmospheric processing on aerosol chemistry and properties
729 at a rural location in the Northeastern U.S., J. Geophys. Res. Atmospheres, 121, 6049–6065,
730 [https://doi.org/10.1002/2015JD024568, 2016](https://doi.org/10.1002/2015JD024568).

731 Zhou, W., Xu, W., Kim, H., Zhang, Q., Fu, P., Worsnop, D.R., Sun, Y., 2020. A review of aerosol chemistry in
732 Asia: insights from aerosol mass spectrometer measurements. Environ. Sci.: Processes Impacts 22, 1616–1653.
733 <https://doi.org/10.1039/D0EM00212G>.

Code de champ modifié